ANALYSIS OF ROCK CRACKING CHARACTERISTICS DURING PYROLYSIS DRILLING

by

Guohua WANG [a*], ***Jun TAN*** [b], ***and Chengxiao LI*** [c]

[a] College of Petroleum and Natural Gas Engineering, Southwest Petroleum University, Sichuan Chengdu, China
[b] College of Petroleum Engineering, Guangdong University of Petrochemical Technology, Guangdong Maoming, China
[c] Drilling and Production Technology Research Institute of CNPC Chuanqing Drilling Engineering Co., Ltd., Guanghan, Sichuan, China

Original scientific paper
https://doi.org/10.2298/TSCI200629322W

Thermal jet rock breaking technology refers to the use of high temperature medium such as supercritical water for a rapid local heating of rocks to break the rocks. Because of the low thermal conductivity of the rock matrix, thermal stress will only form on the rock surface. When the temperature stress exceeds the strength of the rock, micro-cracks will appear in the rock, and continue to expand, resulting in the thermal cracking on the rock surface, which will cause the rock surface to fall off from the body and break the rock. Based on thermal-solid coupling theory, a pyrolysis drilling model was established, and the distribution law of temperature field and temperature stress of bottom hole rock during pyrolysis was obtained by using a finite element method. The results show that during the pyrolysis drilling process, the temperature of the heated part of the rock increases rapidly, producing temperature gradients in radial and axial directions. The expansion of the heated volume is affected by compressive stress in the radial direction, buckling in the axial direction and shear stress. This is very important to the field application of pyrolysis drilling.

Key words: *drilling, thermal jet, thermal cracking, temperature field, temperature stress*

Introduction

Rotary drilling technology, which began around 1900, has become the most widely used method of rock breaking in the oil field [1]. In the 21st century, with the rapid development of modern society and economy, the demand for energy continues to increase. With the increasing difficulty of oil and gas exploitation, the number of deep Wells, complex Wells, and unconventional Wells gradually increases [2]. During the 12th five-year plan period, the change of the number of deep Wells and ultra-deep Wells of PetroChina is shown in fig. 1 [3]. It can be seen from the figure that during the past ten years, the growth rate of deep Wells and ultra-deep Wells has increased by a large margin, almost more than three times.

Accordingly, the increase in well depth leads to higher and higher well construction costs and initial cost input, which greatly limits the development and utilization of both traditional and new energy sources (such as geothermal energy) [4]. This is because the traditional

* Corresponding author, e-mail: wangguohua@swpu.edu.cn

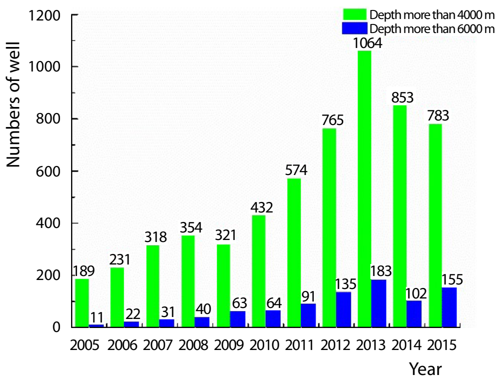

Figure 1. Changes in the number of deep and ultra-deep Wells of PetroChina during the 12th five-year plan period

mechanical rock crushing method relying on drill bits requires a huge amount of energy [5, 6], but only less than 1% of the energy is completely used to break the rock [7]. Most of the energy in this process is converted into noise and heat [8], resulting in a huge waste of energy. On the other hand, various factors in the mechanical drilling process such as operating environment, fluid rheology and formation characteristics [9] may lead to longer non-productive time and lower penetration rates, further increasing drilling costs. Especially in the deep strata, the rock hardness is high, the drilling ability is poor, and the bottom hole energy utilization is low. Since the 12th five-year plan, China national petroleum corporation has systematically tackled the problem of ultra-deep well drilling, continuously improving and optimizing the drilling technology with new technologies and new equipment, but the drilling cost remains high, mainly because of the low rate of mechanical drilling and long drilling cycle, as is shown in tab. 1 [3].

Table 1. Main drilling indicators of the 12th five-year plan in front of Tarim Kuqa mountain

Year	Drilling depth [m]	Drilling cycle [day]	Rate of penetration [mh^{-1}]
2011	6774	478	1.49
2012	6318	330	2.26
2013	6480	270	2.45
2014	6897	320	2.38
2015	7341	330	2.71

The problems of the low drilling speed, short drilling tool life, long drilling cycle and high drilling cost are common in deep well and hard rock drilling. Generally speaking, the cost incurred in the drilling process, that is, the rock breaking stage, has accounted for more than 50% of the total investment in the whole oil and gas production process [10], and its importance is self-evident. Therefore, it is of great significance to the development of society to develop new ways of rock breaking to save cost and reduce capital input, reduce risk factors in the process of rock breaking and protect the environment.

In modern mining engineering, the use of heat to assist the breaking of rock has a history of nearly a century [11, 12]. Since the 1940s, Union Carbide (UC) began to use thermal cracking technology to mine iron flintstone ore, that is, thermal cracking of rocks with high temperature jet tools, and mechanical cutting teeth to break rocks that could not be cracked [13]. With conventional drilling, the relationship between the cost and depth increases geometrically, but with pyrolysis drilling, the relationship between cost and depth is only linear [14]. In 1947, the Linde company used pyrolysis technology as the primary method of rock breaking, which was already capable of producing boreholes thousands of feet deep in iron ore deposits [15]. Compared with traditional mechanical drilling methods, which rely on invading the rock matrix to cut the rock, thermal fracturing means that the rock surface breaks up into small pieces under local heating conditions and breaks off from the rock mass, thus achieving the purpose of breaking the rock. Thermal jet has the advantages of a less energy dissipation and input concentration, while traditional rotary drilling technology has a low energy transfer rate due to the torque loss caused by the drill string [16]. Experiments have proved that the rate of mechanical drilling in granite, quartzite and tight sandstone can reach more than twice that of conventional mechanical drilling by cracking rocks with thermal cracking method [17]. In Los Alamos national laboratory, thermal jet rock breaking tests were conducted, and the drilling rate in granite can reach 6~7.5 m/h, but in new Mexico's geothermal drilling, the drilling rate in granite layer using conventional drilling methods is only 1.2~3 m/h [18]. Browning *et al.* [19] drilled a 330 m deep hole in the granite formation in New Hampshire by thermal cracking, with an average mechanical penetration rate of 15.8 m/h and a maximum of 30 m/h. In general, thermal cracking drilling in hard formations can achieve a mechanical drilling rate of 5-10 times that of conventional rotary drilling [14]. In 1998, the Massachusetts institute of technology [20] proposed the use of supercritical high temperature fluid ($T \geq 375$ °C, $P \geq 22.1$ MPa) [21] to achieve continuous drilling in the formation. In 2005, the USA department of energy conducted research on high temperature fluid pyrolysis drilling as an efficient method for caving underground gas reservoirs [22]. In 2008, Potter Drilling, an American company, co-operated with the Massachusetts institute of technology, conducted an indoor evaluation experiment on fluid thermal cracking technology, designed corresponding equipment and methods [23], and conducted a ground experiment [4] in 2012 to evaluate the rock-breaking effect of thermal cracking. The research results in 2014 have obtained the relevant laws of cuttings morphology and size distribution in the process of pyrolysis and rock breaking of high temperature fluid [24], which can provide a basis for cuttings migration and well cleaning in the process of drilling. In addition, with the thermal jet method, the drilling tool does not come into contact with the rock surface, so there is no such problem as the wear and failure of the drill tool in the traditional mechanical drilling process, which reduces the time to replace the new drill tool. In particular, with the increase of well depth, the superiority of thermal jet drilling method becomes more obvious, greatly reducing the impact of well depth on drilling cost [14].

Therefore, the rock-breaking mode of thermal jet is a drilling method with a very broad application prospect in hard and brittle formations [4]. At present, the implementation of this method is different pipe-lines are set in the drill pipe, and fuel, oxygen and water are injected into the hole along different pipe-lines. The transmission system is shown in fig. 2 [25].

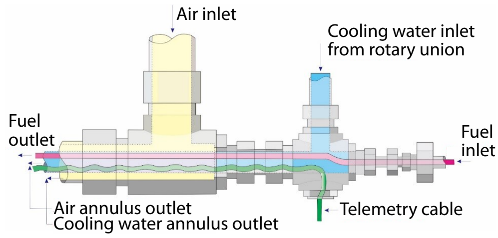

Figure 2. High temperature pyrolysis drilling transmission system

The injected mixture is ignited in the reaction chamber at the bottom of the well so that the fuel reacts with oxygen, resulting in a high temperature and high pressure environment. In this environment, the water will be in a supercritical state ($T \geq 375$ °C, $P \geq 22.1$ MPa) [21], such not only can accelerate the reaction rate of fuel and oxygen, and can form a kind of high temperature of supercritical CO_2 and water medium, inhomogeneous expansion of thermal stress is generated in the rock to rock forming micro-fracture and extending continuously, continuous heating can be realized under the condition of the thermal cracking of the rock broken [26], the whole process can be summarized as:

– when the heat transfer to the rock surface, due to the poor thermal conductivity of rock material, rock surface will produce high temperature stress,

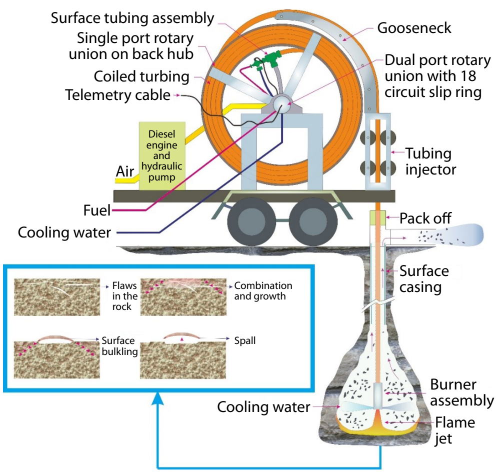

Figure 3. Coiled-tubing-deployed spallation drilling system and the spallation mechanism

– as the temperature stress increases, the volume of the heated part of the rock surface expands, so the whole heated part is affected by compressive stress; when compressive stress is applied to the primary cracks in the rock near the surface, the width of the cracks will expand and the length will be extended; finally, these cracks will merge,
– with the further increase of temperature, the rock surface begins to buckle, and
– the end face of the buckling part is subjected to the action of tensile stress, resulting in the failure of the material, that is, the formation of thermal cracking fragments on the rock surface and then peeling off and detachment from the rock surface.

The pyrolysis drilling system and rock-breaking mechanism are shown in fig. 3 [27].

At present, the research on pyrolysis drilling mainly includes two methods: experiment and numerical simulation. However, the response analysis of rock under thermal shock in the thermal jet process, including the distribution of temperature field and temperature stress in the rock matrix and the crack propagation process, is rarely studied. In this paper, a pyrolysis drilling model is established, and the distribution of field and temperature stress under pyrolysis shock in rock matrix is obtained. On this basis, extended finite element method (XFEM) is used to simulate the crack propagation in rock under thermal shock.

Model building

Model description

During pyrolysis drilling, with the continuous jet of supercritical water from the nozzle to the rock surface, the rock breaks under the action of temperature shock. It is known that the rock matrix is locally heated during pyrolysis drilling, so the supercritical high temperature fluid ejected from the nozzle is taken as the known heat source. Because of the short time interval, the heat loss due to radiation, reflection and other reasons can be ignored. On the calculation area, the high temperature jet nozzle radius and wellbore radius set to 5 mm and 25.4 mm, respectively, [28], because of rock under the action of high temperature pyrolysis time is short, and the rock on the surface of the heated area is far less than the total surface area of the rock, will pit outside as formation, namely in the process of calculation can be treated as an unbounded region. Based on the aforementioned assumptions, a 3-D transient heat conduction model during pyrolysis drilling is established, as is shown in fig. 4.

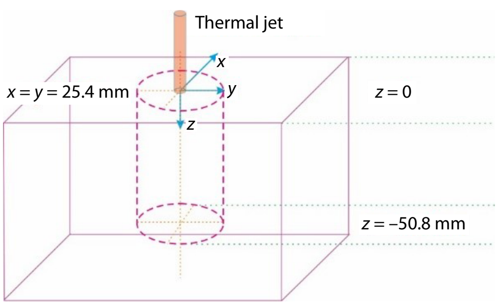

Figure 4. Pyrolysis drilling model

Because of the entire model only subjected to by high temperature jet medium and heat transfer characteristics on the surface of the rock and the influence of the thermal physical properties on the surface of the rock, so the upper surface part of the wellbore in contact with the high temperature jet medium in the model is set as Robin boundary, namely the third kind boundary condition, characterization of forced convection heat transfer between rock surface and supercritical fluid, as shown in fig. 5. The other boundary conditions are set as adiabatic boundary conditions, namely Neumann boundary conditions. This is because the thermal conductivity of the rock matrix is so low that no heat will diffuse to the outer surface of the rock during the calculated time interval [29]. For the convenience of experimental verification, the temperature at time $t = 0$ is taken as the initial temperature and set to room temperature.

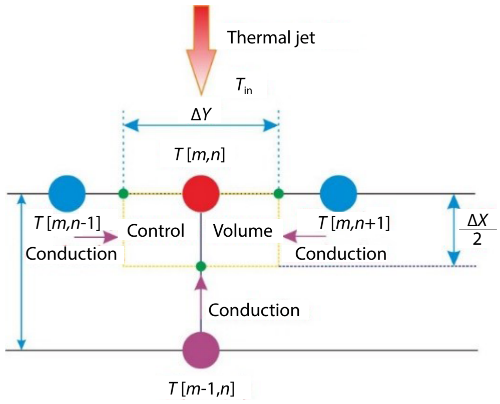

Figure 5. Schematic diagram of pyrolysis jet boundary

Temperature calculation

The thermal conduction control equation [30] is adopted. Because the pyrolysis process takes a short time, the variation of rock properties with temperature is ignored for the sake of simple calculation, and the following equation can be obtained:

$$\rho C_P(T)\frac{\partial T}{\partial t}=\frac{\partial}{\partial x}\left[k(T)\frac{\partial T}{\partial x}\right]+\frac{\partial}{\partial y}\left[k(T)\frac{\partial T}{\partial y}\right]+\frac{\partial}{\partial z}\left[k(T)\frac{\partial T}{\partial z}\right] \tag{1}$$

In order to solve eq. (1), initial conditions and boundary conditions need to be determined in the computational domain.

The initial condition is set as the formation temperature of the rock, expressed by T_0, which can be defined:

$$T(x,y,z,0)=T_0 \tag{2}$$

where T_0 is the for the convenience of comparison with the experimental results in the following text, set to room temperature of 20 °C.

Within the diameter of the thermal jet nozzle, the third type of boundary condition, namely Robin boundary condition, is adopted to set the heat transfer coefficient between the high temperature fluid and the rock surface and the formation temperature where the rock is located (which can be expressed by the initial temperature), which is expressed:

$$-k\left(T\right)\frac{\partial T}{\partial x_i}n_i=h\left(T_{\text{in}}-T_0\right) \tag{3}$$

As is mentioned previously, the formation outside the wellbore is treated as an infinite field. Because the thermal conductivity of the rock matrix is very low, it is generally believed that heat will not spread from the wellbore to the formation in a short time, which can be regarded as an adiabatic boundary. Therefore, the wellbore is set as the second boundary condition, namely Neumann boundary condition:

$$-k\left(T\right)\frac{\partial T}{\partial x_i}n_i=0 \tag{4}$$

The spatial region is discretized into a finite number of volume units, and the temperature, T, distribution of each point in each unit can be obtained by interpolation of the temperature of the unit nodes. Add up the integral of each unit to get:

$$\sum_{e=1}^{M}\int_{\Omega_e}\left[\frac{\partial N_i^e}{\partial x}k_x\frac{\partial \overline{T}^e}{\partial x}+\frac{\partial N_i^e}{\partial y}k_y\frac{\partial \overline{T}^e}{\partial y}+\frac{\partial N_i^e}{\partial z}k_z\frac{\partial \overline{T}^e}{\partial z}\right]\mathrm{d}\Omega-\sum_{e=1}^{M}\int_{\Omega_e}N_i^eQ\mathrm{d}\Omega+\sum_{e=1}^{M}\int_{\Gamma qe}N_i^e\overline{q}\mathrm{d}\Gamma=0 \tag{5}$$

The heat conduction matrix, K, of the element can be expressed:

$$K_{ij}^e=\int_{\Omega_e}\left[\frac{\partial N_i^e}{\partial x}k_x\frac{\partial N_j^e}{\partial x}+\frac{\partial N_i^e}{\partial y}k_y\frac{\partial N_j^e}{\partial y}+\frac{\partial N_i^e}{\partial z}k_z\frac{\partial N_j^e}{\partial z}\right]\mathrm{d}\Omega+\int_{\Gamma_{qe}}hN_i^eN_j^e\mathrm{d}\Gamma \tag{6}$$

The thermal load matrix, f, can be expressed:

$$f_i^e=\int_{\Omega_e}N_i^eQ\mathrm{d}\Omega+\int_{\Gamma qe}hT_fN_i^e\mathrm{d}\Gamma \tag{7}$$

The rock types are set as sandstone, shale and granite, which are commonly encountered in the drilling process. The thermophysical properties and mechanical parameters are shown in tab. 2 [31].

Table 2. Thermophysical properties and mechanical parameters of three kinds of rocks

Rock types	Density [kgm^{-3}]	Young modulus [GPa]	Poisson's ratio	Linear expansion coefficient [K^{-1}]	Specific heat capacity [kJkg^{-1}K^{-1}]	Thermal conductivity [Wm^{-1}K^{-1}]
Sandstone	2000	15	0.12	$5.6 \cdot 10^{-6}$	0.9	4.4
Granite	2700	70	0.3	$8.3 \cdot 10^{-6}$	0.8	2.6
Shale	2850	47	0.2	$19 \cdot 10^{-6}$	1.1	1.3

Thermal stress calculation

Temperature stress is caused by a change in the temperature of an object. In the process of pyrolysis drilling, Thermal Shock effect [32] will cause the temperature to rise rapidly within a short period of time in the jet region, and due to the poor thermal conductivity of the rock, the temperature distribution in the rock is uneven, resulting in a huge temperature gradient in the rock matrix. Therefore, the thermal deformation of each part of the rock are also different, resulting in temperature stress. Under the action of temperature stress, cracks occur in the rock and the cracks continue to expand, resulting in the final cracking of the rock.

When the temperature of an object increases from T_1 to T_2, if its deformation is not restricted, its thermal strain can be calculated:

$$\varepsilon=\alpha\left(T_2-T_1\right)=\alpha\Delta T \tag{8}$$

Granite was selected as the research object, and its thermophysical properties are shown in tab. 2. For the sake of convenience, the rock matrix is still assumed to be continuous, homogeneous, isotropic, and completely elastic. Specifically, in the analysis of temperature stress, the object will not only be subject to external forces and boundary constraints, but also to temperature stress caused by temperature gradient. Under the action of these common factors, the stress state of rock matrix can be analyzed, thus:

– Equilibrium differential equation:

$$\begin{aligned}
&\frac{\partial \sigma_x}{\partial x}+\frac{\partial \tau_{yx}}{\partial y}+\frac{\partial \tau_{zx}}{\partial z}+f_x=0 \\
&\frac{\partial \tau_{xy}}{\partial x}+\frac{\partial \sigma_y}{\partial y}+\frac{\partial \tau_{zy}}{\partial z}+f_y=0 \\
&\frac{\partial \tau_{xz}}{\partial x}+\frac{\partial \tau_{yz}}{\partial y}+\frac{\partial \sigma_z}{\partial z}+f_z=0
\end{aligned} \tag{9}$$

– Geometric equation:

$$\begin{aligned}
\varepsilon_x &= \frac{\partial u}{\partial x} \\
\varepsilon_y &= \frac{\partial \nu}{\partial y} \\
\varepsilon_z &= \frac{\partial w}{\partial z} \\
\gamma_{xy} &= \frac{\partial u}{\partial y}+\frac{\partial \nu}{\partial x} \\
\gamma_{xz} &= \frac{\partial u}{\partial z}+\frac{\partial w}{\partial x} \\
\gamma_{yz} &= \frac{\partial w}{\partial y}+\frac{\partial \nu}{\partial z}
\end{aligned} \tag{10}$$

– Physical equation (representing strain as stress and temperature gradient:

$$\begin{aligned}
\varepsilon_x &= \frac{1}{E}\left[\delta_x-\mu\left(\delta_y+\delta_z\right)\right]+\alpha T_\upsilon \\
\varepsilon_y &= \frac{1}{E}\left[\delta_y-\mu\left(\delta_x+\delta_z\right)\right]+\alpha T'_\upsilon \\
\varepsilon_z &= \frac{1}{E}\left[\delta_z-\mu\left(\delta_y+\delta_z\right)\right]+\alpha T'' \\
\gamma_{xy} &= \frac{2(1+\mu)}{E}\tau_{xy} \\
\gamma_{xz} &= \frac{2(1+\mu)}{E}\tau_{xz} \\
\gamma_{yz} &= \frac{2(1+\mu)}{E}\tau_{yz}
\end{aligned} \tag{11}$$

– The displacement boundary condition is adopted for the boundary condition. Since the heated area on the rock surface is much smaller than its surface area, the wellbore is considered to be surrounded by an infinite far field without displacement. Then the displacement at the wellbore can be written:

$$\begin{aligned}
u_x &= 0 \\
u_y &= 0 \\
u_z &= 0
\end{aligned} \tag{12}$$

By solving eqs. (1)-(11) according to the displacement, the stress is expressed as strain and temperature difference T_υ:

$$\begin{gathered}
\sigma_x = \frac{E}{1+\mu}\left(\frac{\mu}{1-2\mu}e + \varepsilon_x\right) - \frac{E\alpha T_\upsilon}{1-2\mu} \\
\sigma_y = \frac{E}{1+\mu}\left(\frac{\mu}{1-2\mu}e + \varepsilon_y\right) - \frac{E\alpha T'_v}{1-2\mu} \\
\sigma_z = \frac{E}{1+\mu}\left(\frac{\mu}{1-2\mu}e + \varepsilon_z\right) - \frac{E\alpha T''_v}{1-2\mu} \\
\tau_{xy} = \frac{E}{2(1+\mu)}\gamma_{xy} \\
\tau_{yz} = \frac{E}{2(1+\mu)}\gamma_{yz} \\
\tau_{xz} = \frac{E}{2(1+\mu)}\gamma_{xz}
\end{gathered} \tag{13}$$

were e is the volume strain, which can be expressed:

$$e = \varepsilon_x + \varepsilon_y + \varepsilon_z \tag{14}$$

Crack propagation analysis under temperature shock

At present, there are two main views on crack propagation, namely energy balance (such as Griffith theory) and stress field strength (such as Irwin theory). From the aforementioned two views derived from the energy release rate and stress intensity factor the two mechanical quantities. However, when the previous two methods are used to solve the crack propagation under the action of temperature stress, they are limited by the singularity of the crack tip, resulting in the error of the calculation results. The XFEM [33], whose computational grid is independent of the geometric or physical interface inside the structure, can effectively solve various discontinuous problems such as crack propagation, and the crack can extend inside of the element without being affected by the boundary. Therefore, XFEM can be used to analyze the crack propagation evolution in rock matrix under temperature shock. The displacement function of XFEM can be expressed [33]:

$$u^h(x) = \sum_{I\in N} N_I(x)u_I + \sum_{j\in N_{cr}} N_j(x)h(x)a_j + \sum_{k\in N_{tip}} N_k\left[\sum_{l=1}^{4}\psi_l(x)b_{kl}\right] \tag{15}$$

In eq. (15), the first term on the right is the traditional finite element method to describe the node displacement, the second term is used to describe the characteristics of the upper and lower surfaces during the crack propagation process, and the third term is used to describe the singularity of the crack tip in the form of polar co-ordinates.

The $h(x)$ is used to describe the upper and lower surfaces of cracks and can be expressed:

$$h(x) = \begin{cases} 1 & (x - x^*)n \geq 0 \\ -1 & \text{otherwise} \end{cases} \tag{16}$$

where $\psi(x)$ is the used to define the crack tip displacement discontinuity and singularity, polar co-ordinates are used to indicate commonly, can be written:

$$\psi(x)=\left[\sqrt{r}\sin\frac{\theta}{2},\sqrt{r}\cos\frac{\theta}{2},\sqrt{r}\sin\frac{\theta}{2}\cos\frac{\theta}{2},\sqrt{r}\sin\theta\cos\frac{\theta}{2}\right] \tag{17}$$

Equations (16) and (17) are graphically described, as shown in fig. 6. In the figure, the yellow part represents eq. (16), and the purple part represents eq. (17). It can be seen from the figure that eqs. (16) and (17) can completely describe the morphology of a crack.

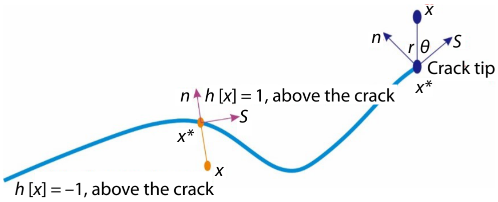

Figure 6. Schematic diagram of crack morphology (*for color image see journal web site*)

Duflot [34] wrote the temperature field as XFEM in the same way, and discretized the temperature at a certain time to obtain:

$$T^h(x)=\sum_{n\in N}N_n(x)T_i+\sum_{j=N_{cr}}N_j(x)h(x)c_j+\sum_{k\in N_{tip}}N_k\psi_2(x)d_k \tag{18}$$

$$T=-\frac{K_T}{\lambda}\sqrt{\frac{2r}{\pi}}\sin\left(\frac{\theta}{2}\right) \tag{19}$$

Therefore, based on the calculation of temperature field and temperature stress in pyrolysis drilling, the obtained temperature stress distribution can be applied to the rock matrix as a pre-stress field, and a crack can be preset inside the rock. In conclusion, a 2-D XFEM model under temperature shock during pyrolysis drilling can be established, as is shown in fig. 7. The red part in the figure shows that the rock is impacted by thermal jet, and a horizontal crack with a length of 7 mm is preset at 6 mm away from the rock surface. Fixed boundaries are adopted around the rock. It is assumed that the rock type is granite and the matrix is isotropic, and its thermophysical properties are shown in tab. 2. The incident temperature of the thermal jet is 600 °C. In the calculation of XFEM, the failure criterion of rock matrix needs to be defined. In general, granite is regarded as a quasi-brittle material, and the maximum principal stress is used as its failure criterion, set as 10 MPa [32]. At the same time, the damage softening criterion of granite was defined and its fracture energy was set at 70 J/m^2 [35]. The initial crack angles were set as 0°, 15°, 30°, 45°, 60°, and 90°, respectively, to study the crack propagation law over time and the influence of the initial crack angle on the crack propagation under thermal shock. After calculation, the crack propagation law of granite subjected to temperature shock during thermal cracking can be obtained.

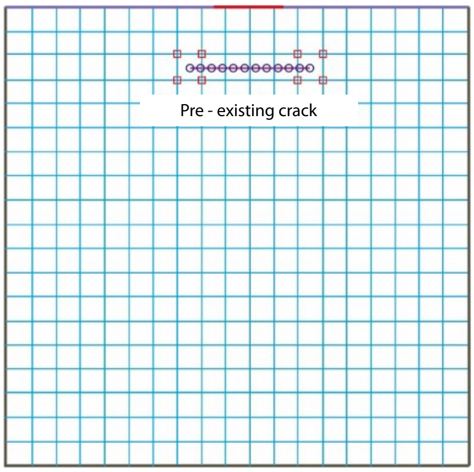

Figure 7. Schematic diagram of XFEM model

Experiments

According to the concept of rock breaking by high temperature jet impact, in order to realize the process of high temperature jet drilling, it is necessary to generate combustion energy to break rock. The whole process includes spraying high temperature medium to the bottom

of the well during the downflow of nozzle and rock breaking under high temperature action. Therefore, the test device shall have the following functions:
– during the test of drilling, the sprinkler head will go down,
– the nozzle does not need to rotate during the test drilling,
– provide combustion conditions and produce high temperature gas,
– it has the control function, and can effectively control the down speed of sprinkler head, the fuel gas used for combustion and the amount of combustion-supporting gas, and
– it has the function of safe operation, and the test device can stop in case of emergency.

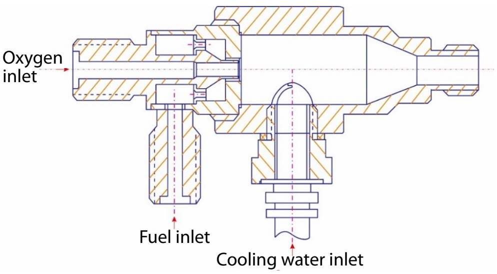

Figure 8. Schematic diagram of combustion chamber

Figure 8 shows the combustion chamber profile of the injector used in the experiment. As is shown in the figure, oxygen and combustible gas are injected into the chamber in a certain proportion make it burn in the chamber. Electric spark ignition method is adopted for ignition, that is, the gas and auxiliary gas entering the ignition chamber are ignited by electric spark to form a combustionrch, and then the gas and auxiliary gas in the combustion chamber of the torch point are used to complete the ignition process. At present, electric spark ignition is widely used in automobile engines and other equipment. The technology is mature. The flow, pressure and mixing ratio of gas and auxiliary gas in the igniter can be adjusted in a wide range, which can meet the requirements of ignition and repeated ignition operation under various working conditions. The bypass is connected to the high pressure cooling water interface, and the high pressure tap water is used instead of the cooling drilling fluid. Figures 9 and 10 shows the experimental system for the combustion temperature test of the whole thermal jet device.

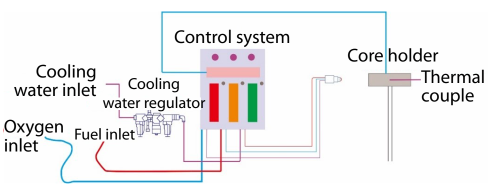

Figure 9. Schematic diagram of thermal jet experimental temperature test

Figure 10. Schematic diagram of thermal jet experimental temperature test nozzle

Results analysis and discussion

Temperature field calculation results

After programming, the cloud diagram of temperature distribution on the XY plane can be obtained as is shown in fig. 11. It can be seen that with the increase of the incident time, the rock temperature in the heat flow region increases rapidly in a short time, but the rate of temperature rise keeps decreasing. However, the thermal conductivity of the rock matrix is poor. Even after the jet time reaches 20 seconds, the high temperature area is still limited to the jet range of the nozzle, thus causing a large temperature gradient inside the rock.

As can be seen from fig. 12, when the jet media just touches the rock surface, there is a huge temperature gradient between the surrounding environment and the rock surface. Within

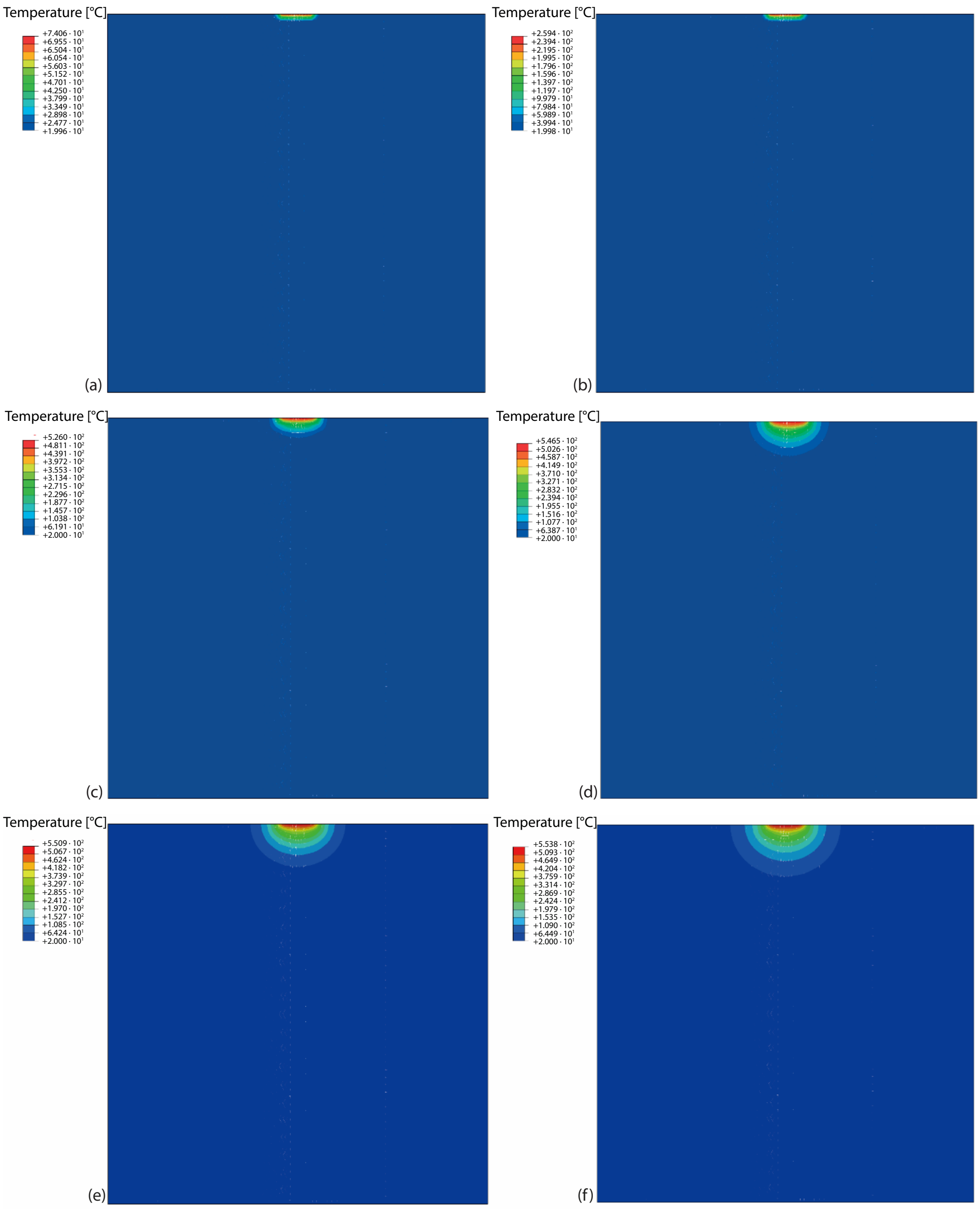

Figure 11. Cloud diagram of temperature field changes with time in pyrolysis drilling (incident temperature is 600 °C; (a) t = 0.01 s, (b) t = 0.1 s, (c) t = 1 s, (d) t = 5 s, (e) t = 10 s, and (f) t = 20 s

0~0.1 second, the temperature at the hole center increases sharply, rising more than 300 °C, and the slope of the curve is almost 90°. Within 1 second, the highest temperature on the rock surface is 90% of the temperature of the hot fluid. Within 10~20 seconds, the slope of the curve

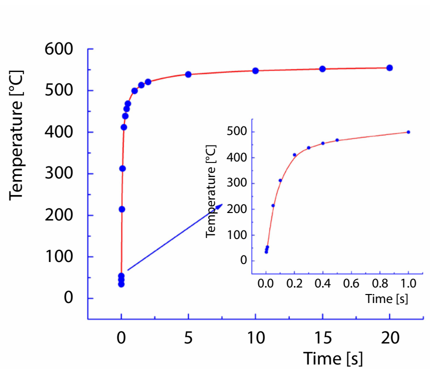

Figure 12. Center temperature of pyrolysis drilling hole changes with time

gradually flattens, and the temperature only increases by about 30 °C. This indicates that during the process of rock heating, the temperature at the borehole center increases with the increase of jet time, but the rate of temperature increase decreases. This is due to the poor thermal conductivity of the rock matrix. With the continuous accumulation of incident heat, the heat exchange efficiency between the incident high temperature fluid and the rock surface is reduced, resulting in a slower and slower increase rate of the rock surface temperature.

Take the XY plane and calculate the radial and axial temperature distribution in the pyrolysis drilling process, respectively. The results are shown in figs. 13 and 14. As can be seen from the figure, as the heating time on the rock surface increases, the temperature in the nozzle diameter area increases rapidly, and the temperature begins to transfer from the center of the well to the surrounding area. But because of the poor thermal conductivity of the rock itself, the rate of temperature propagation is very low. As can be seen from fig. 6, in the radial direction, the center temperature is the highest, and the further away from the hole center, the lower the temperature. With the increase of the heating time, the temperature gradient along the radial direction also increases gradually, that is, the temperature wave range is limited, which can form a large temperature gradient and temperature stress inside the rock, resulting in rock cracking. As can be seen from fig. 7, in the axial direction, the further away from the hole surface, the lower the temperature. With the increase of the heating time on the rock surface, the distance of temperature propagation is further, and the temperature can produce a larger temperature gradient in the axial direction than in the radial direction.

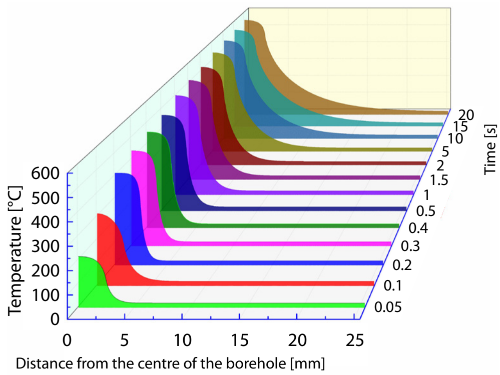

Figure 13. Diagram of radial temperature change with time in pyrolysis drilling

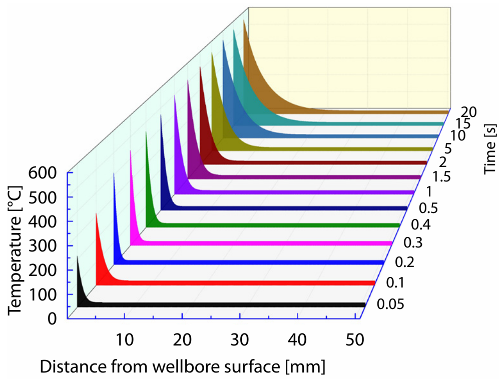

Figure 14. Diagram of axial temperature change with time in pyrolysis drilling

Rock type is the biggest factor influencing the efficiency of high temperature pyrolysis drilling [19]. It can be seen from fig. 15 that rock types have a great influence on the temperature field. The higher the specific heat of rock is, the stronger its ability to absorb heat is, and the higher the surface temperature is in the same heating time. The higher the thermal conductivity of the rock, the stronger its ability to transmit heat, so the wider the temperature spread. The smaller the thermal conductivity of the rock, the slower the temperature transmission speed, the higher the slope of the curve, the larger the temperature gradient can be formed. In general, the thermophysical properties of the three types of rocks shown in the figure are relatively close, but the temperature field is still very different, so the influence of rock types on the thermal cracking effect cannot be ignored.

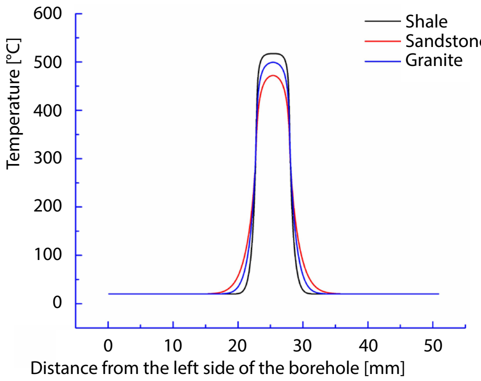

Figure 15. Bottom-hole temperature changes of different rock types (t = 1 s)

Results of temperature stress calculation

During pyrolysis drilling, the rock surface will buckle under the influence of thermal shock and eventually peel off the rock surface. Under the condition of cylindrical co-ordinates, the stress of rock is studied. It can be seen from fig. 16 that during the pyrolysis drilling process, the rock matrix is affected by compressive stress in the radial direction, and the compressive stress at the center of the well is the largest. This is mainly because of the poor thermal conductivity of the rock after being heated, resulting in a large temperature gradient, the volume in the high temperature area expands rapidly, which is caused by the compression of the surrounding rock. The higher the temperature, the greater the volume expansion and the more severe the compression. Therefore, the greater the compressive stress and the farther away from the heated region, the faster the compressive stress decreases. With the increase of the heating time, the compressive stress in the center of the wellbore increases rapidly. The compressive stress can reach the maximum 142.5 MPa within 1 second. Since then, the peak compressive stress hardly increases, and only the area of maximum compressive stress expands with the transfer of heat. Due to the symmetry of the model, it can be seen from fig. 17 that the change of circumferential stress along the hole radius over time has the same characteristics as the change of radial stress.

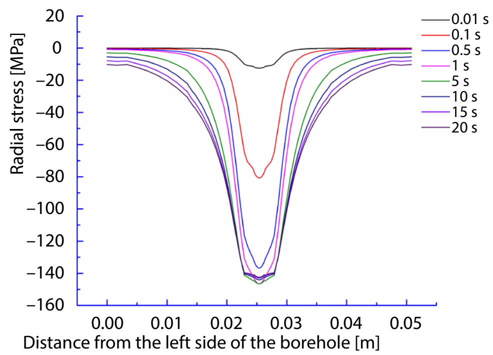

Figure 16. Diagram of radial stress changes with time along the hole radius of pyrolysis drilling, t = 1 s

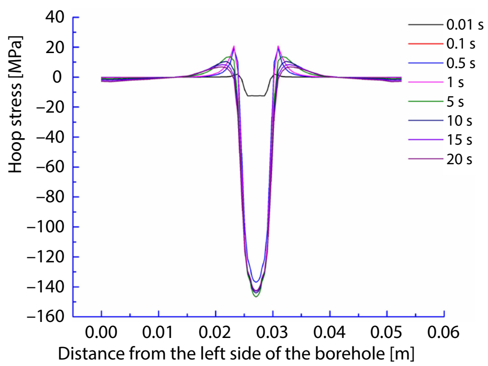

Figure 17. Diagram of stress changes with time along the radius of the hole in the circumferential direction of pyrolysis drilling, t = 1 s

It can be seen from fig. 18 that during the pyrolysis drilling process, the shear force on the rock matrix is symmetrically distributed along the hole radius in the borehole plane, but the absolute value of shear force is very small, less than 0.4 MPa. This is because in the process of heating the rock, assuming that the physical properties of the rock matrix are uniform and isotropic, the rock has the same volumetric strain in all directions along the radial direction, so it is almost unaffected by shear stress on the borehole plane. However, as is shown in fig. 19, it is evident that the rock is subjected to great shear in the axial direction. This is because during the process of rock heating, the rock matrix in the hot zone at the center will buckle when it is squeezed after thermal expansion, resulting in the strain along the Z-axis, that is, perpendicular to the borehole plane, as is shown in fig. 13. The stress state is compared with the strength of the material, and the average shear strength of granite is 10 MPa as its strength limit [13]. It can be seen that rock failure occurs within 0.1 second.

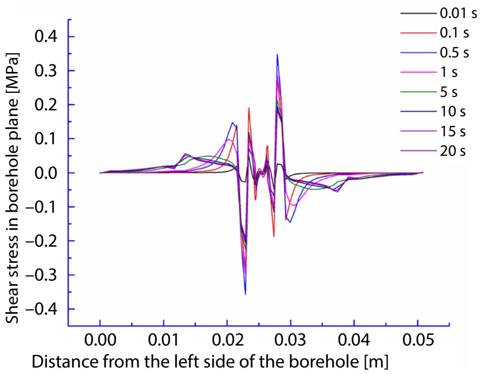

Figure 18. Diagram of shear stress changing with time along borehole radius in pyrolysis drilling hole plane, *t* = 1 s,

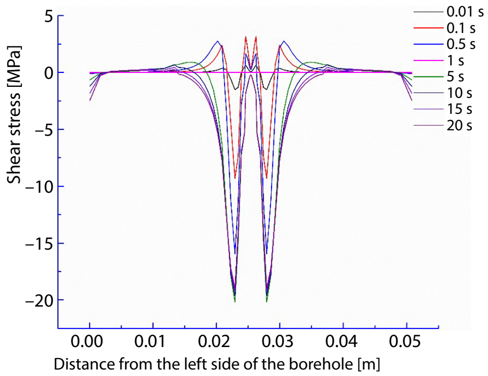

Figure 19. Diagram of axial shear stress changes with time along the radius of the well in pyrolysis drilling, *t* = 1 s,

Crack propagation calculation results

As can be seen from figs. 20 and 21, along the radial direction, buckling occurs almost only on and near the surface of the heated area, while almost no displacement occurs far away from the heated area. The numerical simulation results are in good agreement with the stress and buckling responses of rocks [20].

When the rock is subjected to thermal shock (previous analysis of temperature stress shows that the change of rock surface temperature tends to be flat after 1second heating due to the decrease of temperature difference), the cracks in the rock extend along the direction with the maximum temperature gradient. As can be seen from fig. 22, with the increase of heating time, the area of the crack increases continuously, and the change law of the crack area with time is similar to the change law of temperature stress with time, that is, the change rate is large within the initial heating time, and then decreases gradually as the temperature field tends to be stable.

As can be seen from fig. 23, with the increase of incident temperature, the length and width of cracks in the rock increase. This is because when the incident temperature increases, the temperature difference between the incident temperature and the rock surface increases, and the convection heat transfer becomes stronger. In the same contact time, more heat can be transferred to the rock, so that greater temperature stress and temperature gradient can be generated in the rock matrix, increasing the degree of rock failure.

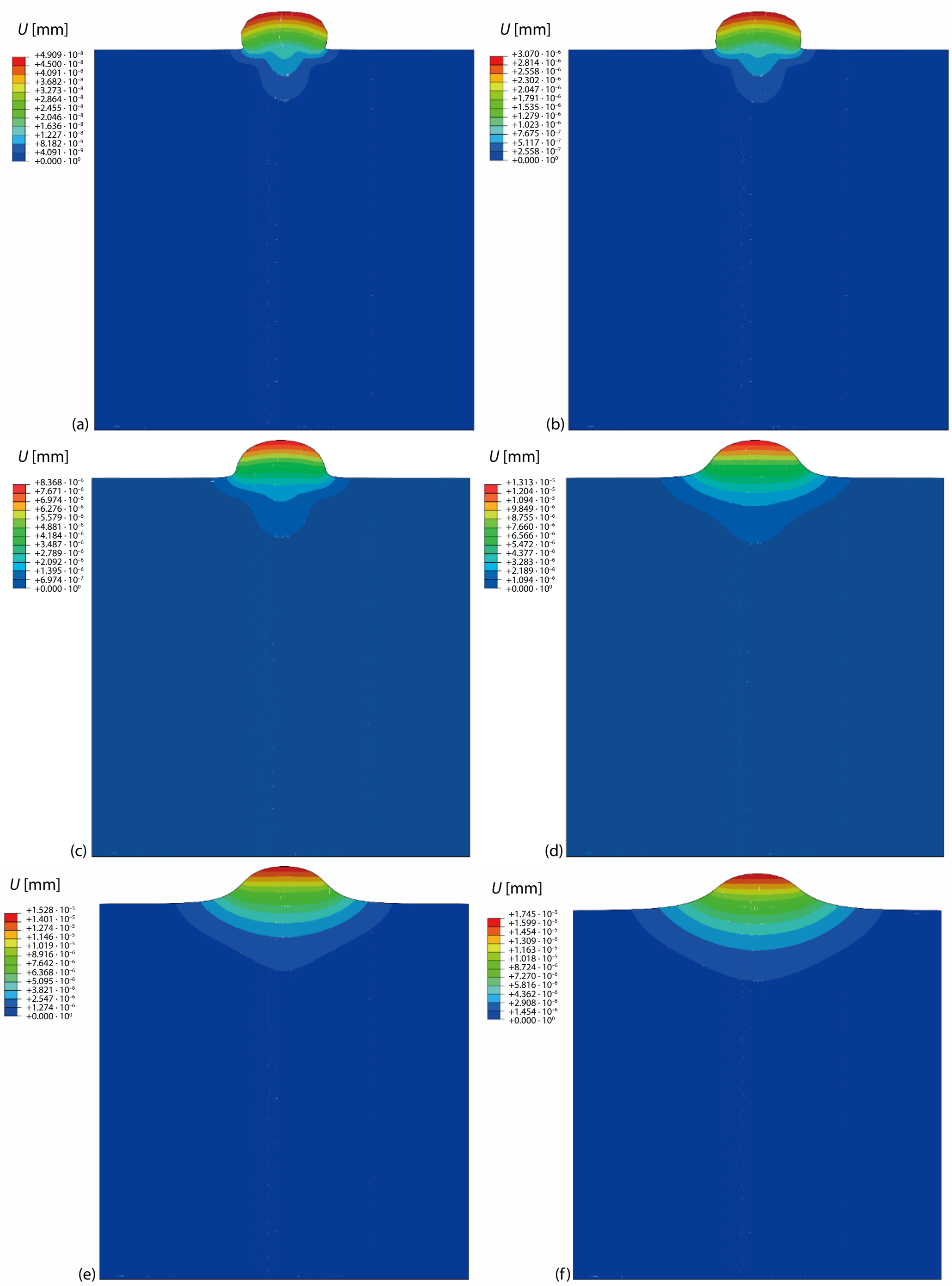

Figure 20. Variation of radial buckling displacement along the borehole with time in pyrolysis drilling; (a) t = 0.01 s, (b) t = 0.1 s, (c) t = 1s, (d) t = 5 s, (e) t = 10 s, and (f) t = 20 s

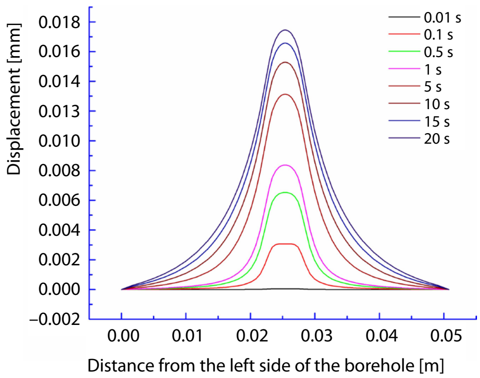

Figure 21. Variation of radial buckling displacement along the borehole with time in pyrolysis drilling

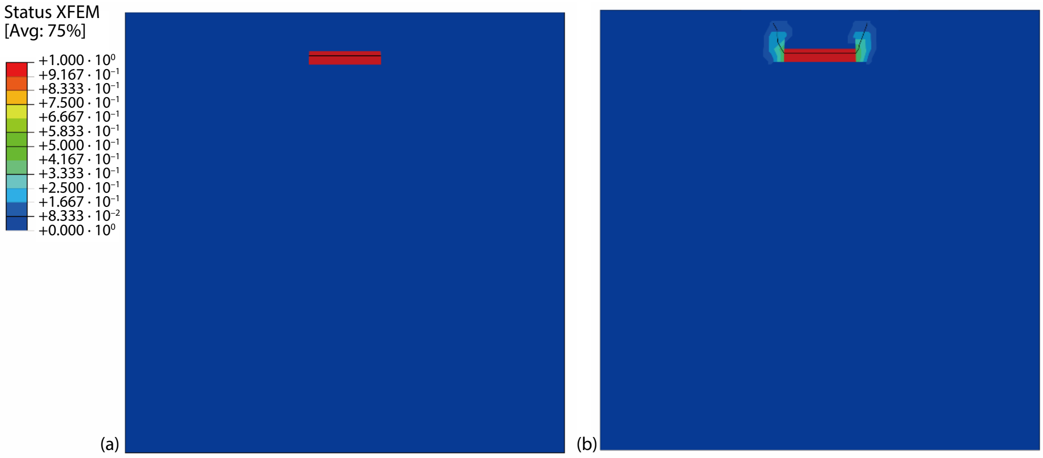

Figure 22. Crack evolution under temperature shock; (a) t = 0 s and (b) t = 1 s

Analysis of experimental results

The jet state diagram with different reactant ratio can be obtained by thermal jet combustion test. The specific ratio of combustion parameters is shown in tab. 3. The experimental results are shown in fig. 24.

Table 3. Combustion parameters table

Injector serial number	Oxygen [Ls^{-1}]	Acetylene [Ls^{-1}]	Total flow [Ls^{-1}]	The water pressure [MPa]
1	16.5	10	26.5	
2	12.5	12.5	25	–
3	25.0	12.0	37	20
4	18.5	18.5	37	20

It can be seen from figs. 24(a) and 24(b) that with the increase of fuel flow, effective jet length increases. However, as the fuel concentration increases, the jet gradually changes to a pure flame form, which is not conducive to rock fragmentation. Therefore, in order to enhance the rock-breaking effect of thermal jet, it is necessary to control the flow ratio of oxidizer and

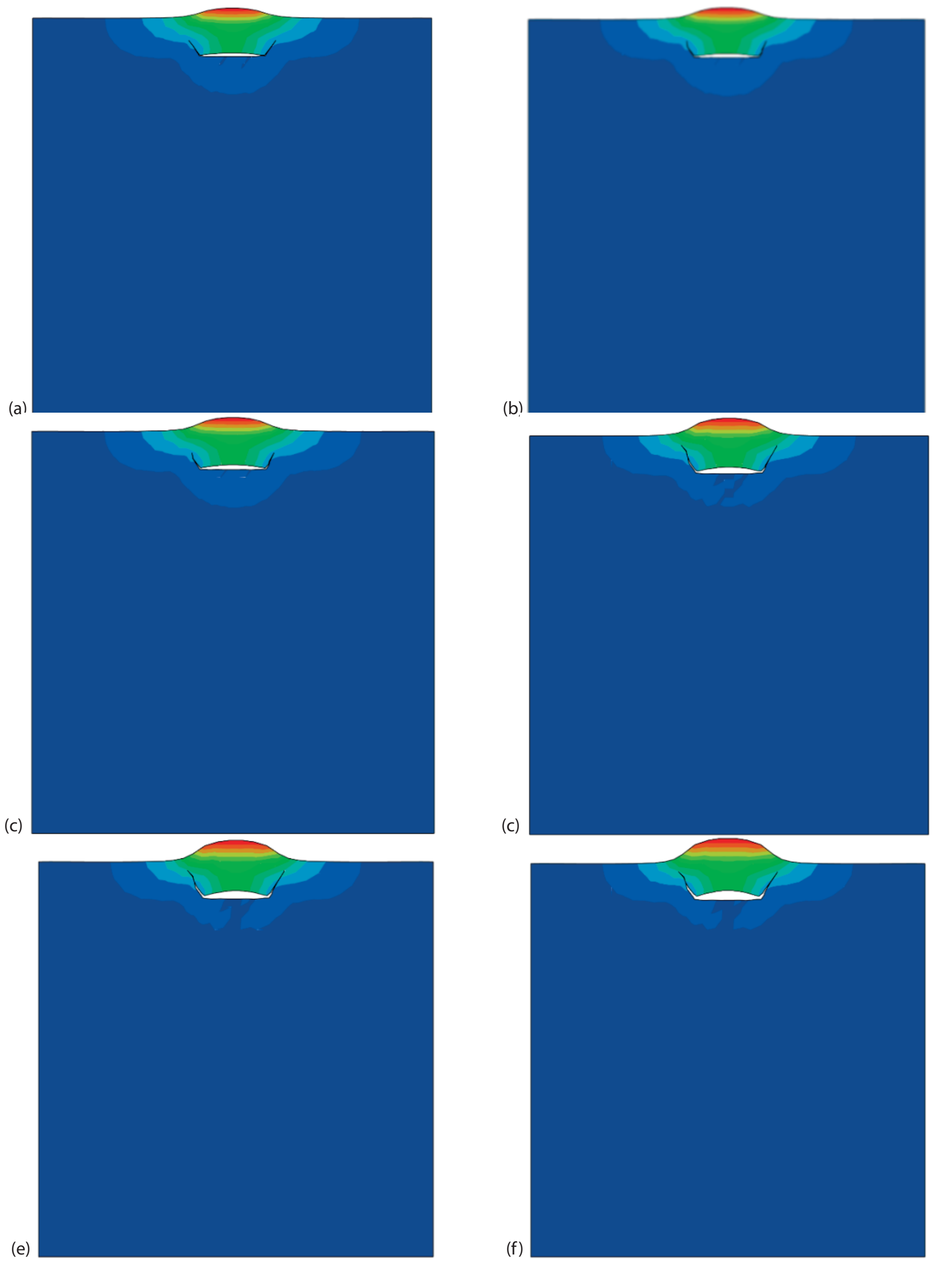

Figure 23. Influence of different incident temperatures on fracture propagation; (a) T = 300 °C, (b) T = 350 °C, (c) T = 400 °C (d) T = 500 °C, (e) T = 600 °C, and (f) T = 700 °C

fuel. Experimental results show that the optimal ratio of fuel to oxidizer flow should be controlled at about 1/3. As can be seen from figs. 24(c) and 24(d), when a certain proportion of water is injected into the combustion chamber, the flame form changes from pure flame to thermal jet, which is more conducive to rock breaking.

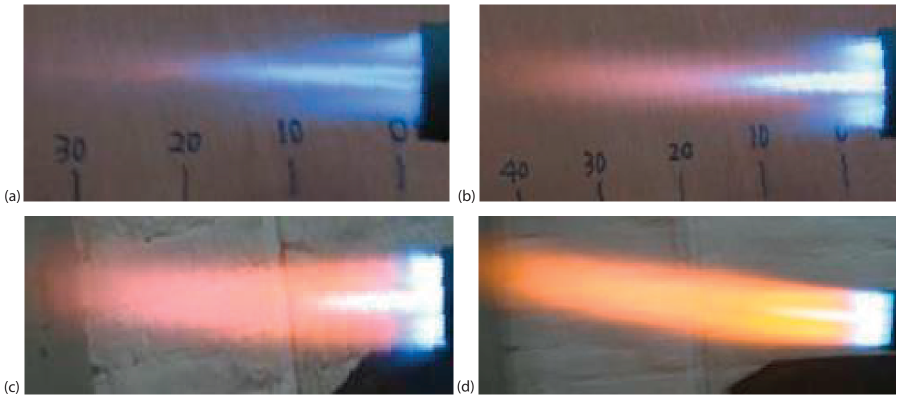

Figure 24. Flame injection diagram with different fuel ratios; (a) No. 1 injector combustion, (b) No. 2 injector combustion, (c) No. 3 injector combustion, and (d) No. 4 injector combustion

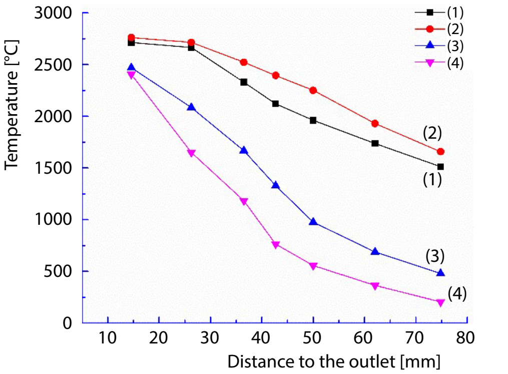

Figure 25. Exit temperature diagram of injection under different reactant ratios

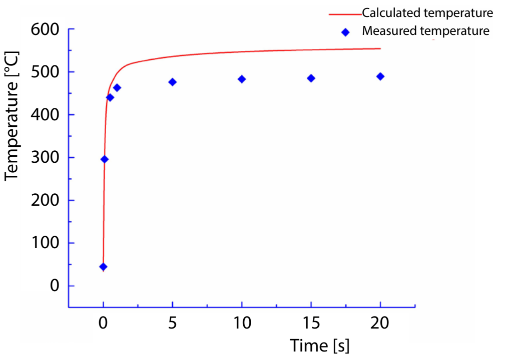

Figure 26. Comparison between experimental data and calculated data of rock center temperature

As is shown in fig. 25, the temperature field test data of the injector are drawn as a comparison diagram. The test results show that the higher the content of acetylene in the fuel, the higher the temperature at the nozzle outlet will be. When the reaction material flow is sufficient, the jet temperature generated by No. 1 and 2 injectors is above 1500 °C, which is enough to meet the needs of thermal cracking and rock breaking, and the jet temperature changes little at different jet distances. After the injection of a certain flow of water, the temperature field generated by the injector rapidly drops below 500 °C, which is an important method to control the temperature of thermal jet. From the nozzle to the point of 60 mm, the outlet temperature of No. 3 and 4 injectors (adding water) decreased linearly. After the spray distance reaches 60 mm, the temperature drops to below 500 °C. If the injection amount of water is increased, the jet temperature can further decrease.

The ratio of fuel and oxidizer was adjusted, and the temperature at the nozzle outlet was controlled to be 600 °C. Granite was used as the experimental sample and the test time was 20 seconds. The temperature at the center point of the rock sample was tested and compared with the calculated result in 4.1, as shown in fig. 26. As can be seen from fig. 26, during the pyrolysis experiment, when the calculation time is very short, the experimental data is in good agreement with the calculated results. With the increase of calculation time, the calculated results deviate from the experimental data. This is because in the process of model calculation, the heat loss of the high temperature fluid in the process of heat transfer to the rock is not considered, including its reflection on the rock surface and heat transfer to the air. However, due to the limited conditions, the experimental rock samples are not placed in the simulated wellbore, but in the air, so there will be errors.

Figure 27 shows the comparison between the experimental temperature measured in the axial direction of the rock matrix and the numerical solution obtained from the pyrolysis model established in section *Results of temperature stress calculation*. It can be seen that the two are in good agreement, and the error is mainly caused by the heat transfer to the air.

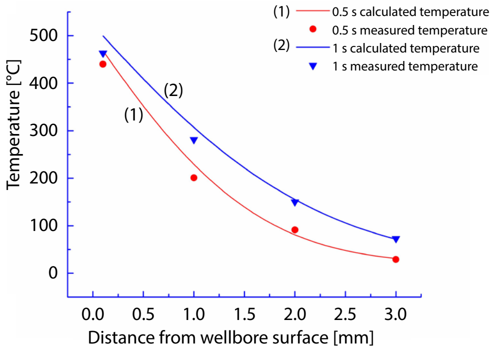

Figure 27. Comparison between experimental data and calculated data of rock center temperature

Conclusions

- During the pyrolysis drilling process, due to the poor thermal conductivity of the rock matrix, the non-uniform temperature field is formed, and the temperature gradient will be generated in the radial and axial directions, thus forming the temperature stress.
- During pyrolysis drilling, the rock matrix is subjected to compressive stress in the radial direction (without considering confining pressure), with the maximum value reaching 142.5 MPa and the maximum compressive stress at the center of the well.
- The heated part in the center of the rock will buckle under the action of high temperature, resulting in strain perpendicular to the plane direction of the borehole, and the shear stress (excluding confining pressure) in this direction is close to 20 MPa, which exceeds the shear strength of the granite, causing the rock surface to peel off from the rock matrix under the action of high temperature.
- Under thermal shock, when there is a preset crack or a weak surface in the rock, the crack will expand along these paths.
- With the increase of fuel flow, effective jet length increases. However, with the increase of fuel concentration, the jet will gradually change into pure flame form. In order to enhance the rock-breaking effect of thermal jet, it is necessary to control the flow ratio of oxidizer and fuel, and the optimal flow ratio of fuel and oxidizer should be controlled at about 1/3. When a certain proportion of water is injected into the combustion chamber, the flame form changes from pure flame to thermal jet, which is more conducive to rock breaking.
- The higher the content of acetylene in the fuel, the higher the temperature at the nozzle outlet. When the reaction material flow is sufficient, the jet outlet temperature generated by the injector is above 1500 °C, which is enough to meet the needs of thermal cracking and rock breaking, and the jet temperature does not change much with the jet distance. After the injection of a certain flow of water, the jet temperature of the injector rapidly drops to below 500 °C, which is an important method to control the temperature of thermal jet.

Nomenclature

C_p – heat capacity at constant pressure, [J°C^{-1}]
h – convective heat transfer coefficient, [10 kWm^{-2}°C^{-1}]
k – thermal conductivity, [Wm^{-1}°C^{-1}]
T – temperature, [°C]
n – the unit vector at x^*, [–]
n_i – unit outward normal vector, [–]
$T_{\rm in}$ – incident temperature of high temperature fluid, [°C]
X – integral point, [–]
x^* – the point closest to x on the fracture surface, [–]

Greek symbols

γ_{ij} – shear strain, [–]
ε_i – normal strain, [–]
ρ – density, [kgm^{-3}]
τ_{ij} – shear stress, [MPa]

References

[1] Simon, R., Comparing the Rotary with Potential Drilling Methods, *Journal of Petroleum Technology, 10-11* (1958), 11, pp. 28-30
[2] Rajnauth, J., Is It Time to Focus on Unconventional Resources, *Advances in Petroleum Exploration & Development*, *4* (2012), 2, pp. 37-45
[3] Wang, H., *et al*., Technologies in Deep and Ultra-Deep Well Drilling: Present Status, Challenges and Future Trend in the 13th Five-Year Plan Period – in Chnese (2016-2020), *Natural Gas Industry*, *37* (2017), 4, pp. 1-8
[4] Walsh, S. C., *et al*., Grain-Scale Failure in Thermal Spallation Drilling, Report No- LLNL-CONF-523558, Lawrence Livermore National Laboratory, Livermore, Cal., USA, 2012
[5] Tromans, D., Mineral Comminution: Energy Efficiency Considerations, *Minerals Engineering*, *21* (2008), 8, pp. 613-620
[6] Schwechten, D., Milburn, G. H., Experiences in Dry Grinding with High Compression Roller Mills for End Rroduct Quality below 20 Microns, *Minerals Engineering*, *3* (1990), 1, pp. 23-34
[7] Fuerstenau, D. W., Abouzeid, A. Z. M., The Energy Efficiency of Ball Milling in Comminution, *International Journal of Mineral Processing*, *67* (2002), 1, pp. 161-185
[8] Toifl, M., *et al*., The 3-D Numerical Study on Microwave Induced Stresses in Inhomogeneous Hard Rocks, *Minerals Engineering*, *90* (2016), 6, pp. 29-42
[9] Adeniji, A. W., The Applications of Laser Technology in Downhole Operations – A Review, *Proceedings*, International Petroleum Technology Conference, Doha, Qatar, 2014
[10] Shen, Z., *et al*., Analysis on New Development and Development Trend of Worldwide Drilling Technology, *Journal of China University of Petroleum*, *33* (2009), 4, pp. 64-70
[11] Holman, B. W., Heat Treatment As An Agent in Rock Breaking, *Trans IMM*, *26* (1926), 219, pp. 382-397
[12] Yates, A., Effect of Heating And Quenching Cornish Tin Ores Before Crushing, *Trans IMM*, *28* (1918), 41, pp. 918-929
[13] Teodoriu, C., Cheuffa, C., A Comprehensive Review of Past and Present Drilling Methods with Application Deep Geothermal Environment, *Proceedings*, 36th Workshop on Geothermal Reservoir Engineering Stanford University, Stanford, Cal., USA, 2011
[14] Tester, J. W., *et al*., Prospects for Universal Geothermal Energy from Heat Mining, *Science & Global Security*, *5* (1994), 1, pp. 99-121
[15] Calaman, J. J., Rolseth, H. C., *Technical Advances Expand Use of Jet-Piercing Process in Taconite Industry*, American Rock Mechanics Association, New York, USA, 1962
[16] Sheppard, M. C., *et al.*, Designing Well Paths to Reduce Drag and Torque, *SPE Drilling Engineering*, *2* (1987), 4, pp. 344-350
[17] Potter, R., *et al*., Laboratory Study and Field Demonstration of Hydrothermal Spallation Drilling, *GRC Transactions*, *34* (2010), 52, pp. 249-262
[18] Dey, T. N., *et al*., Methods for Increasing Drilling Performance of the Thermal Spallation Drilling System, *Rock Drilling*, *9* (1985), 8, pp. 1205-1231
[19] Browning, J., *et al*., Recent Advances in Flame Jet Working of Minerals, *Proceedings*, 7th Symposium on Rock Mechanics, State College, Pen., USA, 1965
[20] Potter, R. M., Tester, J. W., Continuous Drilling of Vertical Boreholes by Thermal Processes: Including Rock Spallation and Fusion, American Rock Mechanics Association, New York, USA, 1998
[21] Wagner, W., The IAPWS Formulation 1995 for the Thermodynamic Properties of Ordinary Water Substance for General and Scientific Use, *Journal of Physical & Chemical Reference Data*, *31* (2002), 2, pp. 387-435

[22] Song, X., et al., Numerical Analysis on the Impact of the Flow Field of Hydrothermal Jet Drilling for Geothermal Wells in a Confined Cooling Environment, *Geothermics*, *66* (2017), Mar., pp. 39-49
[23] Wideman, T. W., *et al*., Methods and Apparatus for Thermal Drilling, Patent No. US20100089577A1, Potter Deilling Inc., USA, 2010
[24] Walsh, S. D. C., *et al*., Size Dependent Spall Aspect Ratio and Its Effects in Thermal Spallation, *International Journal of Rock Mechanics & Mining Sciences*, *70* (2014), 9, pp. 375-380
[25] Dreesen, D., Bretz, R., Coiled-Tubing-Deployed Hard Rock Thermal Spallation Cavity Maker, Department of Energys National Energy Technology Laboratory, Huston, USA, 2005
[26] Augustine, C. R., Hydrothermal Spallation Drilling and Advanced Energy Conversion Technologies for Engineered Geothermal Systems, *Massachusetts Institute of Technology*, *109* (2009), 4, pp. 49-68
[27] Rothenfluh, T., Heat Transfer Phenomena of Supercritical Water Jets in Hydrothermal Spallation Drilling, Ph. D. thesis, ETH, Zurich, Switzerland, 2013
[28] Song, X., *et a*l., Numerical Analysis of Characteristics of Multi-Orifice Nozzle Hydrothermal Jet Impact Flow Field and Heat Transfer, *Journal of Natural Gas Science & Engineering*, *35* (2016), A, pp. 79-88
[29] Meier, T., *et al*., Numerical Investigation of Thermal Spallation Drilling Using An Uncoupled Quasi-Static Thermoelastic Finite Element Formulation, *Journal of Thermal Stresses*, *39* (2016), 9, pp. 1138-1151
[30] Koskelainen, L., The CONFID-A General Finite Difference Program for Heat Conduction Problems, *Proceedings,* Numerical Methods in Thermal Problems, Swansea, Wales, 1979
[31] Li, M., *et al*., Simulation of Thermal Stress Effects in Submerged Continuous Water Jets on the Optimal Standoff Distance during Rock Breaking, *Powder Technology*, *320* (2017), 123, pp. 47-59
[32] Lu, T., *et al*., The Thermal Shock Resistance of Solids, *Acta Materialia*, *46* (1998), 13, pp. 4755-4768
[33] Moes, N., *et al*., A Finite Element Method for Crack Growth without Remeshing, *International Journal for Numerical Methods in Engineering*, *46* (1999), 1, pp. 131-150
[34] Duflot, M., The Extended Finite Element Method in Thermoelastic Fracture Mechanics, *International Journal for Numerical Methods in Engineering*, *74* (2010), 5, pp. 827-847
[35] Ai, H. A., Ahrens, T. J., Numerical Modelling of Shock-Induced Damage for Granite under Dynamic Loading, AIP Conference Proceedings, *AIP*, *845* (2006), 1, pp. 1431-1434

Paper submitted: June 29, 2020
Paper revised: September 7, 2020
Paper accepted: September 28, 2020